Concentrating solar collectors integrated with low CO_2 emissions ultra supercritical power plants

Vittorio Tola, Mario Petrollese, Mario Cascetta and Daniele Cocco

University of Cagliari, Department of Mechanical, Chemical and Material Engineering, Cagliari (Italy)

Abstract

This paper focuses on the evaluation of the potential benefits arising from the integration of concentrating solar systems with coal-based Ultra Supercritical (USC) power plants with post-Combustion CO_2 Capture (PCC). In this study, the USC-PCC plant was integrated with a concentrating solar field with or without a thermal energy storage section. Different collector technologies (parabolic trough and linear Fresnel) and heat transfer fluids (direct steam generation and molten salts) were analyzed and compared. The performance of both solar field and power plant were evaluated by means of specifically developed models, by using data sets of a typical meteorological year for two sites in Italy and Morocco. A preliminary cost analysis was finally carried out.

Keywords: CSP plant, USC, CO_2 capture, parabolic trough, Linear Fresnel

1. Introduction

Worldwide, the Concentrating Solar Power (CSP) plants installed capacity is around 5000 MW, generated using parabolic troughs (83 %), solar towers (13 %), linear Fresnel reflectors (3.4 %) and single dish engines (0.02 %) [1]. Moreover, it is rapidly increasing with about 4000 MW of additional capacity under construction or development. [2]. Nowadays, different technologies and configurations are available for solar field (parabolic trough, linear Fresnel, solar tower and solar dish systems), power block (steam Rankine and ORC, Stirling engines, combined cycles, etc.), heat transfer fluid (thermal oil, molten salts, steam, etc.) and thermal energy storage (TES) systems (active, passive, two-tank, thermocline, etc.) [3,4]. Currently, parabolic trough collectors (PTC) are the most commercially proven technology for the solar field. Linear Fresnel collectors (LFC) are a viable alternative, despite a lower optical efficiency but requiring less land availability and capital costs [5,6]. Thermal oil is usually used as heat transfer fluid (HTF), but the maximum allowable temperature for these fluids is limited to about 400°C. For this reason, one of the main R&D activities in this field aims to overcome this limit by replacing it with Molten Salts (MS) or by using Direct Steam Generation (DSG) solar plants [7,8].

One of the most interesting options is represented by the integration of the solar field with a conventional power plant fed by fossil fuels through hybrid CSP plants [9]. A solar hybrid plant can utilize the existing infrastructure of a conventional power plant, thereby, reducing the investment cost and, consequently, the costs of electricity production. In addition, solar contribution in fossil plants allows to reduce fuel consumption and therefore CO_2 emissions [10]. Hybrid CSP plants can be found in North Africa and Middle East countries, where solar system have been integrated with combined cycles [11,12]. Moreover, with the aim to reduce CO_2 emissions, conventional power plants should require their integration with Carbon Capture and Storage (CCS) systems. In particular, coal-based steam plants require Post-Combustion CO_2 Capture (PCC) processes based on chemical absorption, especially with amine-based solvents, leading to a remarkable net efficiency penalty [13], in the order of 10-11 percentage points for the usual target of most CCS projects (90% CO_2 removal) [14,15]. Since low and medium temperature thermal energy can easily be produced by solar radiation, in recent years, several interesting options for integrating solar energy and CCS technologies have been studied aiming to mitigate the energy penalty generated by the large heat consumption required for solvent regeneration [16]. In particular, two main approaches are proposed: the first is the production of low-pressure steam for the solvent regeneration process (at about 130-140 °C). The advantage of using this approach is that, for a given fossil fuel input, steam production from solar energy reduces the extraction from the low-pressure (LP) turbine increasing its power output. The second

doi:10.18086/swc.2017.04.15 Available at http://proceedings.ises.org

approach is the production of high or intermediate pressure steam for the high-pressure (HP) and intermediate-pressure (IP) turbines. In this case, for a given fossil fuel input, steam production from solar energy raises the mass flow of the steam turbines and therefore increases the overall power output. Obviously, from a thermodynamic point of view, the latter is undoubtedly the preferred approach [17,18], although the best option also depends on climatic conditions and solar collector technology. The integration of solar systems both based on parabolic trough collectors and linear Fresnel collectors with PCC has been studied [18–20], demonstrating that solar integration improves the economic feasibility of CCS, especially for decreasing collector costs and increasing CO_2 emission prices [21,22].

In this framework, the present study evaluates the performance improvements of an Ultra Super Critical (USC) steam power plant with PCC integrated with concentrating solar collectors. USC systems represent the state of the art in the field of coal fired power plants, with conversion efficiencies above 45-46%, more than 5 percentage points greater than those of conventional steam power plants [23]. Firstly, the USC-PCC plant was integrated with a solar field based on LFC or PTC with DSG, without considering a thermal energy storage. Subsequently, the results were compared with those of an USC-PCC plant integrated with PTC using Molten Salts (PTC-MS) as HTF and a two-tank direct TES. The comparative analysis aims to evaluate the increase in USC-PCC energy production and global efficiency due to the solar energy contribution by considering two different locations: Sardinia (Italy) and Morocco. Finally, a preliminary cost analysis was also included, evaluating the levelized cost of energy (LCOE).

2. Configuration and performance of the solar field

As mentioned, a solar field based on parabolic trough (PTC) or linear Fresnel collectors (LFC) is considered in this paper. For both options, PTC and LFC collector line includes several modules connected in series and the different lines of linear collectors are connected in parallel to achieve the required thermal power output. Two different solutions based on direct steam generation or molten salts are compared. Table 1 reports the main geometrical and performance parameters assumed in this study [24].

Table 1 - Main characteristics of solar collectors.

	LFC (DSG)	PTC (DSG)	PTC (MS)
Module length/ width	44.8/16.56 m	100/5 m	100/5 m
Focal length F	7.4 m	1.8 m	1.8 m
Module collecting area A_C	513.6 m^2	470.3 m^2	470.3 m^2
Modules per line	16	8	8
Reference optical efficiency	0.665	0.745	0.745
Cleanliness efficiency	0.98	0.98	0.98
Inlet/outlet steam conditions (p=80bar)	175°C/500°C	175°C/500°C	175°C/500°C
Receiver thermal losses	$0.056\Delta T+2.13E\text{-}4\Delta T^2$ (EVA) $0.013\Delta T+6.251E\text{-}10\Delta T^4$ (SH)	$0.056\Delta T+2.13\ E\text{-}4\Delta T^2$ (EVA) $0.013\Delta T+6.251E\text{-}10\Delta T^4$ (SH)	Forristall model [25]

The performance of PTC and LFC are evaluated on a yearly basis and compared by means of a specifically developed simulation model starting from hourly data of Direct Normal Irradiation (DNI), solar position, air temperature and wind speed. Firstly, the actual thermal power incident into the receiver $\dot{Q}_{INC}$ is calculated according to the following equation:

$$\dot{Q}_{INC} = DNI \cdot A_C \cdot \eta_{OPT,R} \cdot IAM \cdot \eta_{END} \cdot \eta_{SHD} \cdot \eta_{CLN} \quad \text{(eq. 1)}$$

where $\eta_{OPT,R}$ is the reference optical efficiency, IAM the Incidence Angle Modifier, η_{END} the end-loss optical efficiency, η_{SHD} the shadow efficiency and η_{CLN} the surface cleanliness efficiency. Figure 1 shows the two IAM components in function of the longitudinal and transversal components θ_L and θ_T of the solar incidence angle θ. End loss optical efficiency is evaluated in function of collector length, focal height and longitudinal component θ_L. Shadow efficiency is considered only for the PTC cases and is evaluated in function of the distance between module rows and collector width.

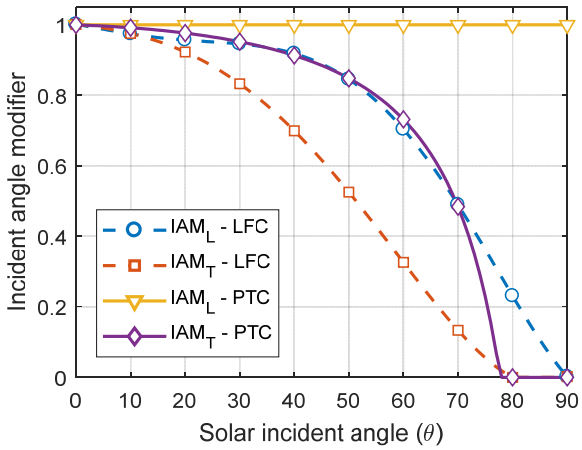

Figure 1 - Longitudinal and transversal IAM components

The thermal power $\dot{Q}_{SF}$ actually transferred to the HTF is calculated by applying the receiver energy balance:

$$m_R \frac{\partial h}{\partial t} + \dot{Q}_{REC,L} - \dot{Q}_{INC} = -\dot{Q}_{SF} = \dot{m}_{HTF}(h_{IN} - h_{OUT}) \quad \text{(eq. 2)}$$

Where the first term considers the thermal capacity of the HTF inside the tube and $\dot{Q}_{REC,L}$ represents the receiver thermal losses evaluated according to the specific correlations reported in Table 1 (ΔT is the temperature difference between the HTF temperature and the ambient temperature). A more detailed description of the simulation model can be found in [26]. Finally, a solar field control is introduced and the mass flow rate $\dot{m}_{HTF}$ is adjusted to meet the design point value of the loop outlet enthalpy. The latter is set to produce steam at 500 °C and 80 bar. For the DSG case, the overall steam production directly feeds the USC plant and the rated steam mass flow rate and the solar field aperture area are determined by setting a desired solar field power output under nominal conditions.

In case of molten salts as HTF, a direct two-tank TES system is considered: one tank stores the hot fluid while the other holds the exhausted cold fluid. The TES system is modelled by considering the mass and energy balance of each tank, as reported in the following equations:

$$\frac{\partial m_{TES}}{\partial t} = \dot{m}_{HTF,IN} - \dot{m}_{HTF,OUT} \quad \text{(eq. 3)}$$

$$m_{TES} \frac{\partial h_{TES}}{\partial t} = \dot{m}_{HTF,IN} h_{HTF,IN} - \dot{m}_{HTF,OUT} h_{TES} - \dot{Q}_{TES,L} \quad \text{(eq. 4)}$$

where m_{TES} is the HTF mass stored in the tank, $\dot{m}_{HTF,IN}$ and $\dot{m}_{HTF,OUT}$ are the inlet and outlet mass flow rate respectively, h_{TES} is the average HTF enthalpy inside the tank, $h_{HTF,IN}$ is the inlet HTF enthalpy and $\dot{Q}_{TES,L}$ are the TES thermal losses due to a not perfect insulation of the tanks. The HTF stored in the hot tank is then used to produce steam in a heat exchanger, simulated by considering a constant pinch point temperature difference (set to 10°C) and by applying a steady-state energy balance:

$$\dot{m}_{HTF}(h_{HTF,IN} - h_{HTF,OUT}) = \dot{m}_S(h_{S,OUT} - h_{S,IN}) \quad \text{(eq. 5)}$$

Where $\dot{m}_S$ is the steam mass flow rate, $h_{S,OUT}$ and $h_{S,IN}$ are the outlet and inlet steam enthalpy respectively. Therefore, thanks to the introduction of a TES system, the PTC-MS configuration slightly differs from the DSG case, as the steam mass flow rate produced is constant and does not depends on the solar energy availability. The thermal storage capacity (C_{TES}) is here expressed in terms of equivalent full-load hour of TES, which indicates the number of hours that the thermal storage section can supply energy to the heat exchanger to produce steam at nominal conditions. Moreover, in order to better exploit the TES storage an increase of solar field aperture area respect to the rated one is often recommended. Solar multiple (SM) is therefore used to represent the actual solar field thermal power as a multiple of the solar field reference thermal power. It is worth noting that the solar

multiple in case of DSG is always equal to one in this study. Two locations characterized by different DNI availability are considered in order to compare the energy performance and the cost-effectiveness of the solar field in different weather conditions. In particular, a site with a high DNI availability (Ouarzazate, Morocco, 2444 kWh/m²y) and one with a lower DNI (Cagliari, Sardinia, Italy, 1720 kWh/m²y) are evaluated. The data set for a typical meteorological year was obtained from the Meteonorm software, including DNI, solar azimuth and elevation, air temperature, relative humidity and wind velocity. Table 2 reports the main meteorological data of the chosen sites and the corresponding design conditions assumed for the solar field.

Table 2 - Meteorological data for the sites of Italy and Morocco and solar field design assumptions.

		Italy	Morocco
Available DNI	kWh/m^{2}y	1720	2444
Average ambient temperature	°C	17.2	18.8
Average wind velocity	m/s	3.96	3.80
Design DNI	W/m^2	800	900
Design elevation/azimuth angles	°	74.2/0.0	82.5/0.0
Design ambient temperature	°C	22.5	30.0

For both sites, Table 3 reports the main performance of a single line in terms of reference thermal power output and reference efficiency, as well as annual thermal energy production and average efficiency (the ratio of annual thermal energy production and annual available DNI), considering both LFC and PTC with DSG and PTC-MS. A decrease of about 9 percentage points in the reference efficiency and 17 percentage points in the average efficiency is observed in the LFC case compared to PTC with DSG. This is mainly due to the lower reference optical efficiency of the linear Fresnel collectors together with the effect of the transversal IAM, which is not present in the parabolic trough collectors. A reduction of about 3 percentage points in the reference efficiency is also detected by using PTC with molten salts instead of DSG, due to the higher HTF average temperature inside the receiver tube and the consequent increase of the receiver thermal losses. A more important decrease is observed in the annual performance due to both the higher receiver thermal losses and the higher thermal inertia of the molten salts. A reduction of 2-3 percentage points from Italy to Morocco cases is finally observed, because of different weather conditions and solar elevation. This difference rises up to 9 percentage points in the PTC-MS case. In fact, this case is characterized by a higher thermal inertia of the molten salts involving in the solar field due to the presence of a TES section. Consequently, a great increase of the energy spent to warm the molten salts in the first morning up to the nominal conditions occurs.

Table 3 - Performance of a single LFC and PTC line.

		LFC		PTC		PTC-MS	
		Ita	Mor	Ita	Mor	Ita	Mor
Collecting area	m^2	8217.6	8217.6	3762.4	3762.4	3762.4	3762.4
Reference thermal power	MW	4.030	4.720	2.118	2.469	2.020	2.370
Reference efficiency	%	61.30	63.82	70.36	72.92	67.11	70.00
Solar energy availability	GWh/y	14.12	20.08	6.47	9.19	6.47	9.19
Thermal energy production	GWh/y	5.85	8.91	3.77	5.66	2.53	4.43
Average efficiency	%	41.43	44.37	58.3	61.55	39.1	48.2

3. Configuration and performance of the USC plant with PCC

USC power plants are characterized by very hard operating conditions, reaching maximum steam pressures higher than 30 MPa and maximum steam temperatures up to 600-620 °C [27]. In recent years, several R&D studies focused on a further increase of the steam pressure and temperature with the aim of reaching overall plant efficiency as high as 50% [28]. The achievement of higher temperatures and pressures is closely related to the use of suitable advanced materials to withstand the harshest operating conditions [29,30]. A medium size plant (in the order of 450-500 MW_e) has been considered for this study. This size is lower than typical modern USC plant, but better matches with the integration with the solar field. The reference plant configuration is based on a superheated and double reheat steam cycle with ten regenerative steam extractions and four steam turbines: a very high-pressure turbine (VHPT), a high-pressure turbine (HPT), an intermediate pressure turbine (IPT) and a low-pressure turbine (LPT). Figure 2 shows a simplified scheme of the USC power plant.

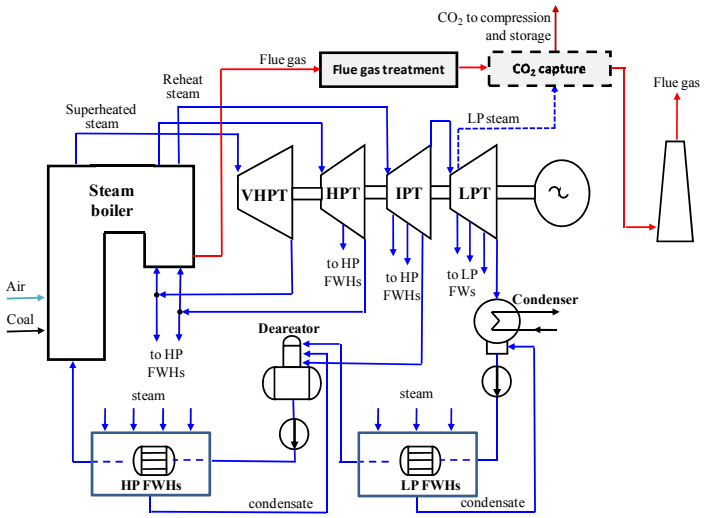

Figure 2 - Simplified scheme of the USC plant.

Performance of the plant have been assessed referring to a commercial coal, characterized by a carbon fraction slightly higher than 0.65 and a lower heating value of 25.03 MJ/kg. A coal power input of 1.0 GW was imposed. The plant is equipped with both a conventional flue gas cleanup (FGC) section (including a selective catalytic reduction denitrification system, baghouse filters and a low temperature flue gas desulphurization system) and a low temperature CO_2 removal section, based on a post-combustion chemical absorption process with amine-based solvents (MEA 30%wt), including an absorption and a regeneration column. To match CO_2 transport and storage requirements, the CO_2 removal section is also integrated with a conditioning and compression section to provide a high pressure (11 MPa) and high purity (99.7% by volume) CO_2 flow.

As in modern USC units, a maximum pressure of 33.5 MPa has been assumed, leading to a superheated (SH) steam pressure at the VHPT inlet of about 30 MPa. A minimum pressure of 4.2 kPa has also been assumed at the condenser. Superheated and reheat (RH) steam temperatures of 600 and 620 °C have been assumed, respectively. High temperature of the steam extraction allows to reduce to -1.5 °C the minimum temperature difference inside the high-pressure feedwater heat exchangers, whereas such a difference increases up to 1.5 °C inside the low-pressure feedwater heat exchangers. A deaerator pressure of 0.8 MPa has been assumed. Table 4 reportes the main characteristics of the plant and Table 5 summarizes its overall performance. The very high pressure of the first steam extraction (slightly lower than 15 MPa) allows to increase water temperature upstream of the economizer above 335 °C. The reference USC plant (without CCS) attains a net power output of about 465 MW with a corresponding net efficiency of 46.64%. The integration with the CO_2 removal section largely reduces the USC performance, mainly due to the large steam extraction (at about 4 bar) for solvent regeneration and to the power required by the CO_2 compression process.

Table 4 - Main characteristics of the USC plant.

Coal chemical power input	MW	1000
SH/RH1/RH2 steam temperatures	°C	600/620/620
SH/RH1/RH2 steam pressures	MPa	30.0/13.5/5.4
Cycle maximum pressure (boiler feedwater pump)	MPa	33.5
Cycle minimum pressure (condenser)	kPa	4.2
Deaerator pressure	MPa	0.8
BOP loss as steam turbine power fraction		0.02
High/low pressure heat exchangers minimum ΔT	°C	-1.5/1.5
MEA mass fraction	%	30
CO_2/MEA molar ratio		0.28
Reboiler specific thermal energy	MJ/kg_{CO2}	3.72

Table 5 - Overall performance of the USC plant.

		NO-CCS	CCS
Coal chemical power input	MW	1000	1000
- Steam turbines	MW	516.4	439.7
- Pumps	MW	16.1	16.1
Steam cycle output	MW	500.0	423.6
- Aux. absorptions and mechanical losses	MW	19.4	16.1
- Generator losses	MW	5.2	4.4
Gross power output	MW	475.4	403.1
- FGC section absorptions	MW	9.0	9.0
- CO_2 capture and compression	MPa	-	32.4
Net power output		466.4	361.7
Net efficiency		46.64	36.17
Plant availability	h/year	8760	8760
Energy production	GWh/year	4085.6	3168.5
CO_2 emissions	Mt/year	3.00	0.300
CO_2 specific emissions	g/kWh	734.3	94.7

In particular, a CO_2 removal efficiency of 90% requires about 320 MW_t, halving the LPT mass flow and reducing the USC power output by about 70 MW. This remarkable penalty combined with the power requirements of the CO_2 capture and compression section causes a noteworthy power output reduction of about 105 MW. Overall, the introduction of the PCC process reduces the energy production by about 25% and the USC efficiency by about 10.5 percentage points (from 46.6% to 36.2%). Obviously, the CO_2 specific emissions greatly benefit from the introduction of the CO_2 capture and compression section (decreasing from about 735 to about 95 g/kWh).

4. Performance of the integrated CSP-USC-PCC plant

To mitigate the energy penalty generated by the large heat consumption required for solvent regeneration, the USC-PCC plant has been integrated with concentrating solar collectors in a CSP-USC-PCC plant. The hybridization occurs through the production of intermediate pressure steam (80 bar and 500°C). The water is extracted downstream of the feedwater pump, it is pre-heated, vaporized and superheated in the solar field and then reintroduced downstream of the high-pressure turbine before entering in the second reheater. In particular, when solar energy is available, the IP steam produced by the solar field increases the mass flow rate of both IP and LP steam turbines allowing a greater power production but leading also to an off-design operation mode of the USC plant with a corresponding efficiency penalty. Moreover, the steam production from solar field causes both an increase of the LP turbine outlet pressure and a rise in the condenser thermal load, therefore, leading to a higher cooling water requirement or higher cooling water outlet temperature. Figure 3(a) shows the pressure and the condenser mass flow rate (the latter in percentage with respect to design conditions) in function of the ratio between solar field power output ($\dot{Q}_{SF}$) and fuel power input ($\dot{Q}_{USC}$). The condenser mass flow greatly increases with solar contribution and, therefore, in order to avoid an excessive increase in the condenser thermal load, a maximum value of the power ratio equal to 0.2 was considered in this study. The increase in steam pressure and mass flow leads to corresponding changes in the turbine power output owing to the sliding pressure operating mode of the steam turbine. Obviously, the USC-PCC-CSP net power output increases with the solar contribution and annual average performance of the power plant are greatly influenced by annual DNI availability. However, the USC power plant operates without solar energy integration for a large share of the annual operating hours, as concentrating solar collectors require a minimum available DNI (100-150 W/m^2). Moreover, during most of the solar field operating hours, the DNI is below its design value. Therefore, in the case of direct steam generation, the USC plant operates at reference conditions when no solar production occurs, while it operates in off-design conditions with the introduction of IP steam from solar field, with a corresponding cycle efficiency penalization. On the other hand, the use of molten salts as heat transfer fluid allows the introduction of a thermal storage at relative low costs. In this case, the steam production from the solar field is constant along the day with an important increase of the operating hours at on-design conditions.

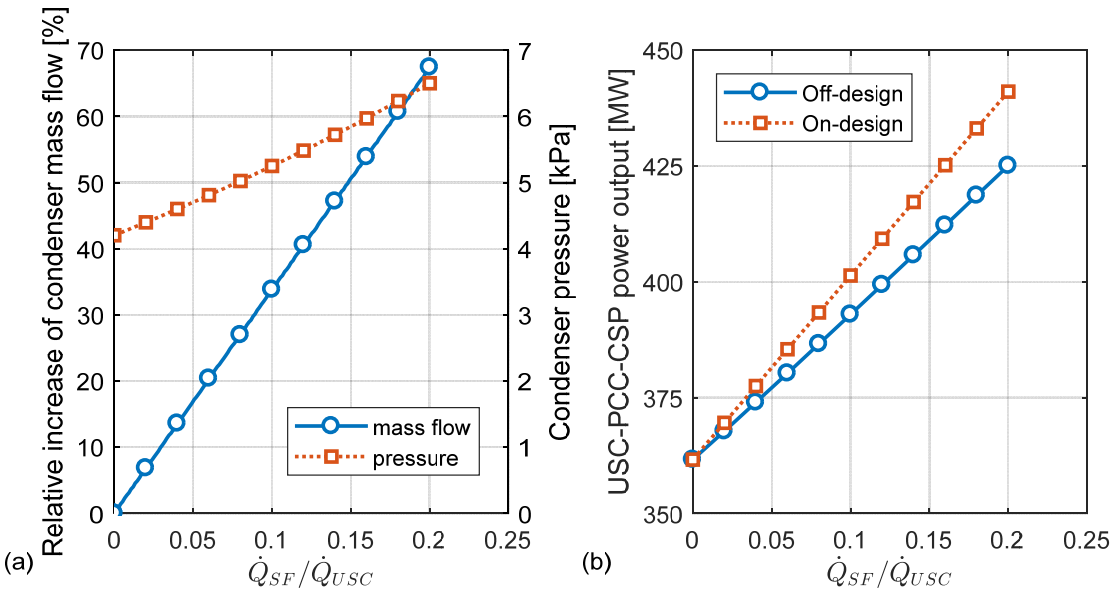

Figure 3 – (a) Relative increase of the condenser mass flow, condenser pressure and (b) power output of the USC-CCS-CSP plan as a function of the ratio between solar field power output and fuel power input.

The advantages in terms of efficiency and, thus, of net power output by working at on-design conditions instead of off-design is shown in Figure 3(b) as a function of the ratio between solar field power output and fuel power input. Figure 4(a) shows the annual performance of the system in terms of USC net energy production as a function of the ratio between the solar field power output and fuel power input in case of direct steam generation or molten salts as HTF (storage capacity equal to 4 hours and solar multiple equal to 1). The USC net energy production linearly increases with the solar contribution for all cases, and, as expected, the highest values are reached by adopting parabolic trough collectors. By referring to the Morocco case, an increase of 0.715 GWh in annual USC energy production for an increase of 1 MW of solar field reference thermal power is detected for PTC with DSG, 0.840 GWh/MW_{CSP} for the PTC-MS case and 0.590 GWh/MW_{CSP} for LFC solar field. Similar trends are observed by referring to the Italian site, although the lower DNI availability results in a lower solar contribution of 0.550 GWh/MW_{CSP}, 0.545 GWh/MW_{CSP} and 0.450 GWh/MW_{CSP} for the PTC-DSG, PTC-MS and LFC configurations, respectively. It is worth noting that for a given value of solar contribution, the overall collecting area increases by using LFCs instead of PTCs and by considering an Italian location instead of a Moroccan one.

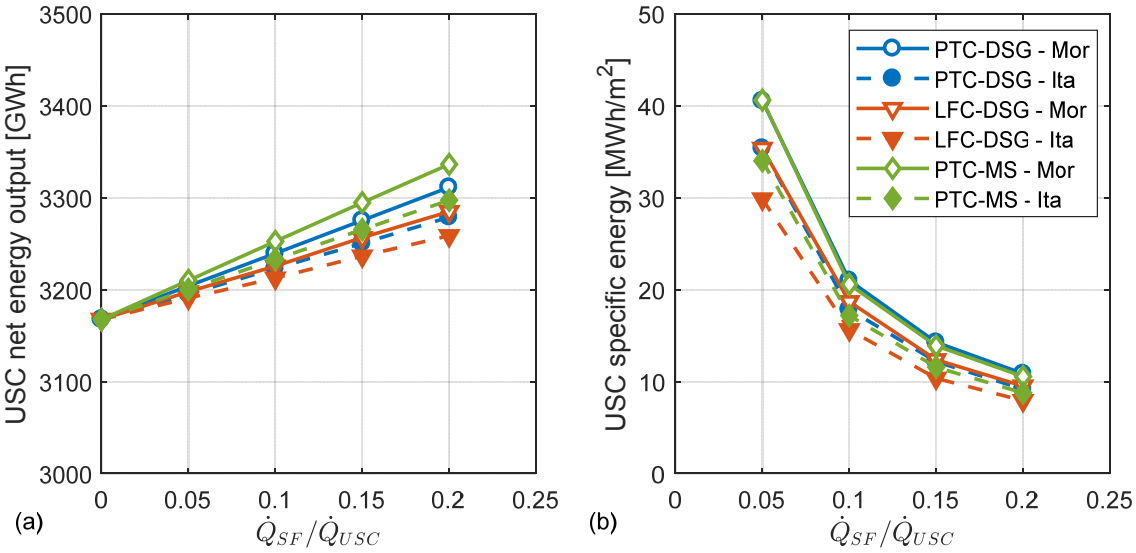

Figure 4 – (a) Annual USC-PCC-CSP energy production and (b) specific energy production as a function of the ratio between solar field power output and fuel power input.

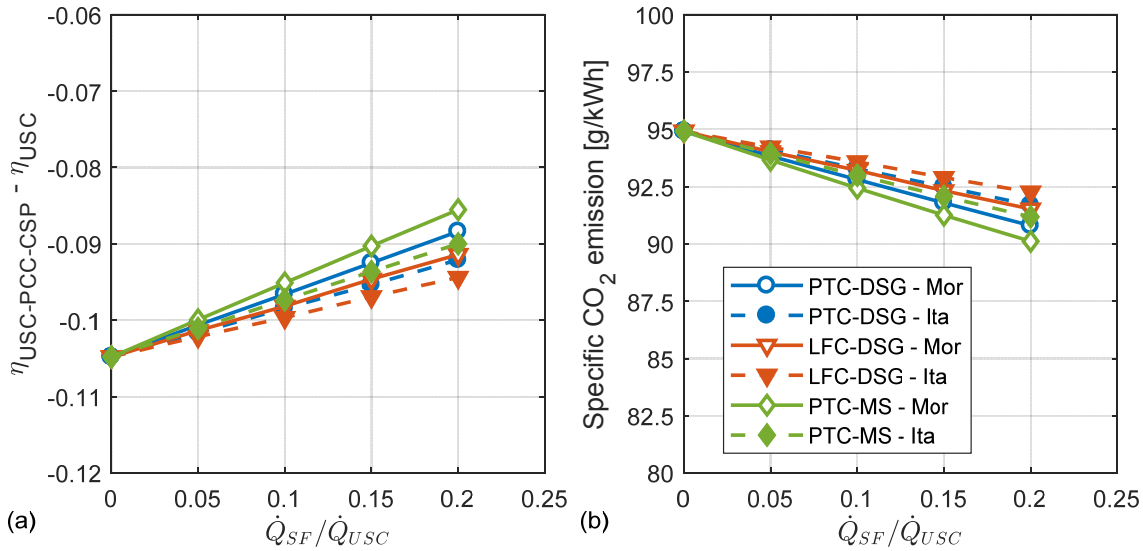

Figure 5 – (a) USC efficiency decrement and (b) specific CO_2 emissions as a function of the ratio between solar field power output and fuel power input.

For instance, for a solar contribution equal to 0.2, the overall collecting areas are about 304750 m^2 (81 loops) and 357430 m^2 (95 loops) for PTC in Morocco and Italy respectively, while the LFC solar field is characterized by a collecting area of 345140 m^2 (43 loops) in Morocco and 410880 m^2 (50 loops) in Italy. For this reason, Figure 4(b) depicts the specific annual energy production in terms of energy produced per unit area of solar field. The figure shows a marginal difference between the use of DSG and molten salts by referring to the Moroccan case. In fact, although as reported in Table 3 the average efficiency of the solar field using molten salts was lower than the use of PTC-DSG, they are substantially balanced by the higher USC efficiency resulting from the constant steam mass flow rate production of the solar field. On the other hand, the drop in solar field performance detected for the Italian case by using molten salts as HTF is predominant and the use of the PTC-DSG achieves the highest specific energy production. The main benefits arising from a solar integration are shown in Figure 5:

- the efficiency penalty due to the CO_2 removal section are partially balanced by the steam generation from the solar field (Figure 5(a));
- a further reduction of the specific CO_2 emissions is achieved thanks to the increase of annual energy production due to solar field without any further production of carbon dioxide (Figure 5(b)).

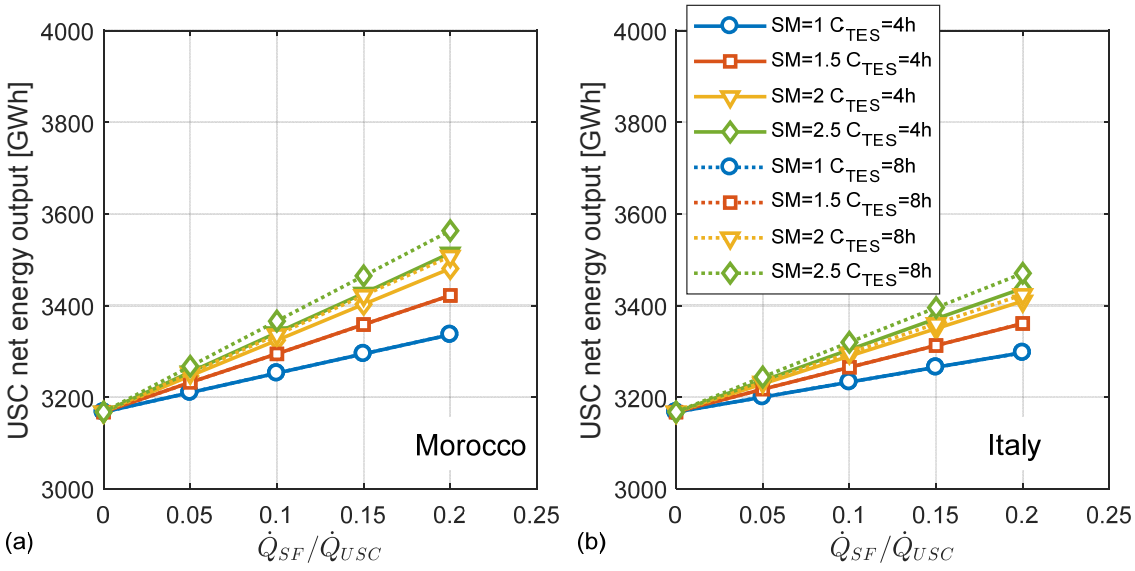

Figure 6 - Annual USC-PCC-CSP energy production as a function of the ratio between solar field power output and fuel power input for the Molten Salts case.

Both these performance indexes follow a linear increment with the increase in the solar field power output.
As mentioned, one of the advantages of introducing a TES system is the possibility to time shift the production of the solar field. In other words, with a TES system it is possible to increase the time of steam feeding to the USC by keeping a constant mass flow rate. As mentioned, other two important design parameters for the molten salts case are the storage capacity and the solar multiple. Figure 6 shows the annual energy production of the USC plant as a function of the solar contribution for different combinations of solar multiple and TES capacity. For solar multiples lower than 2, a TES capacity higher than 4 full-load hours do not introduced any benefits in terms of rising in energy production, independently form the plant location. On the other hand, with the rise in the solar multiple value, a higher storage capacity is required to store the surplus of energy produced by the solar field, especially during summer days. In particular, the increase of the TES capacity from 4 to 8 hours in Morocco results in an increase of about 15% of the annual steam production.

5. Preliminary economic analysis

A preliminary economic analysis was carried out to compare the energy production cost of the reference USC plant (with and without PCC) and the solar assisted configurations. In fact, the increment in the energy production with the solar integration also results in a rise of capital and operating costs. The economic analysis is based on the determination of the levelized cost of electricity (LCOE) for the various configurations considered. The LCOE was calculated by means of the following equation:

$$\mathrm{LCOE} = \frac{\mathrm{TCI_{USC}} + \mathrm{TCI_{PCC}} + \mathrm{TCI_{CSP}} + \sum_{n=1}^{N}\left(\mathrm{C_F} + \mathrm{C_{O\&M,USC}} + \mathrm{C_{O\&M,CSP}}\right)(1+\mathrm{i})^{-n}}{\sum_{n=1}^{N}\mathrm{E_E}(1+\mathrm{i})^{-n}} \qquad \text{(eq. 6)}$$

Where $\mathrm{TCI_{USC}}$, $\mathrm{TCI_{PCC}}$ and $\mathrm{TCI_{CSP}}$ are the total capital cost investment of the USC plant, PCC system and the CSP section (including solar field costs and, if present, TES costs) respectively, $\mathrm{C_F}$ is the annual cost of the fuel, $\mathrm{C_{O\&M,USC}}$ and $\mathrm{C_{O\&M,CSP}}$ are the operating and maintenance costs for the USC-PCC plant and solar section, $\mathrm{E_E}$ is the annual energy production, i is the annual interest rate and N is the expected operating lifetime.

Table 6 - Cost assumptions of the USC-PCC plant, solar field and TES section.

USC specific capital investment	1300 €/kW	Solar field specific cost	100-300 €/m^2
PCC specific capital investment	1170 €/kW	Piping specific cost	30 €/m^2
O&M cost of USC (% of TCI)	3%	Land cost	10 €/m^2
O&M cost of PCC (% of TCI)	2.5%	TES specific cost (only MS case)	625 €/m^3
Coal price	75 €/t	Molten salts cost	0.93 €/kg
Engineering cost (% of direct cost)	20%	O&M cost of solar section (% of TCI)	1.5%
Contingency cost (% of direct cost)	2%	Annual interest rate	7%
Insurance annual cost (% of TCI)	1%	Operating lifetime	20

Table 6 reports the main cost assumptions. In particular, the assumption of specific costs for the USC-PCC plant are taken according to [15], and for the CSP plant according to [31]. The solar field specific cost is not constant but ranges in the interval 100-300 €/m^2. In fact, the present economic analysis aims to evaluate the minimum capital cost of the solar field that allows to produce electricity at a lower LCOE than the reference USC-PCC plant. For a solar integration of 20% (that is the ratio between solar field power output and fuel power input equal to 0.2), Figure 7(a) shows the LCOE for the six different cases analyzed as a function of the solar field specific cost, as well as the LCOE obtained without considering any solar integration. Obviously, a linear increase of the LCOE is observed with the increase of the solar field specific costs. The LFC case always attains higher values of LCOE than PTC and a decrease of the solar field cost of about 60 €/m^2 should occurs to becomes competitive with PTC solar fields. The LCOE with solar integration in the Italian case always exceeds the LCOE of the USC-PCC plant even for the lowest solar field specific costs. On the other hand, the solar integration becomes cost effective for a solar field cost lower than 180 €/m^2 for the PTC-DSG case. The use of molten salts and the introduction of a TES section, despite the enhancement in annual energy production, increase the capital and operating costs and result less profitable than the direct steam generation.

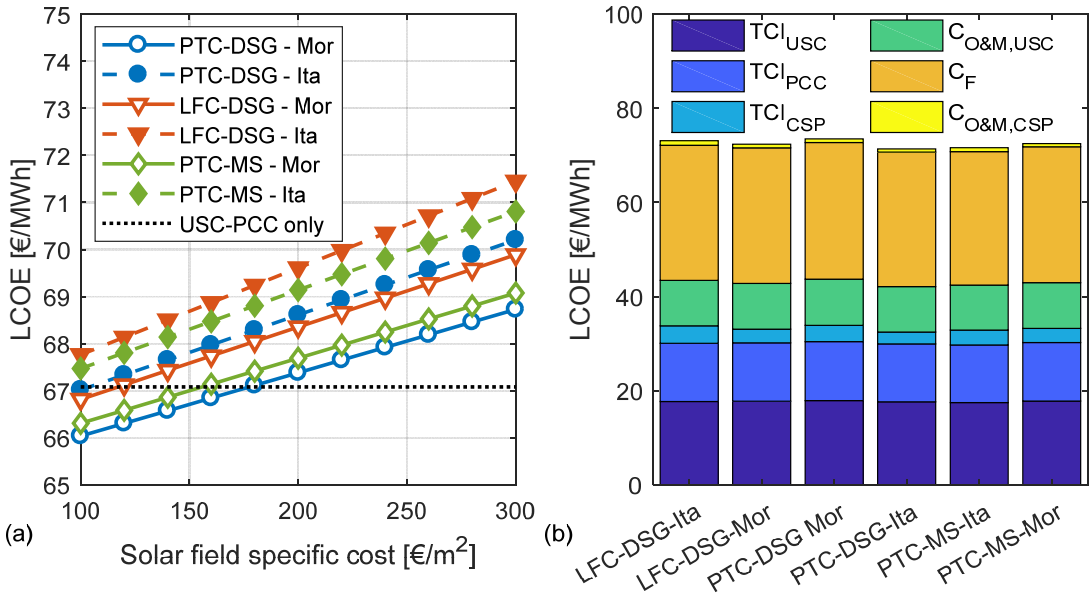

Figure 7 – (a) Levelized cost of electricity as function of the solar field specific cost and (b) influence of capital and operating costs on the determination of the LCOE.

It is worth noting that the influence of the solar field costs on the overall plant costs is marginal. As shown in Figure 7(b), by assuming a solar field specific cost of 200 €/m^2, the capital cost for solar integration contributes for about 5% of the overall LCOE while O&M costs of the solar section are lower than 1%. Finally, Figure 8 shows the levelized cost of energy in case of molten salts as HTF and different values of solar multiple and TES capacity. The figure demonstrates the not profitability to increase the storage capacity beyond 8 hours independently from the location, as the excess energy that cannot be stored due to the complete charge of the TES section is minimal (only for few summer days in case of C_{TES}=4h). Consequently, the rise in capital costs due to higher storage and HTF costs is not properly balanced by the increase in the energy production. On the other hand, an increment of the solar multiple to 1.5 could be a cost-effective solution if the solar field specific cost drops to 160 €/m^2 in the Morocco case. In this case, the benefits arising from a higher energy production becomes preponderant compared to the corresponding increment of the solar field capital costs.

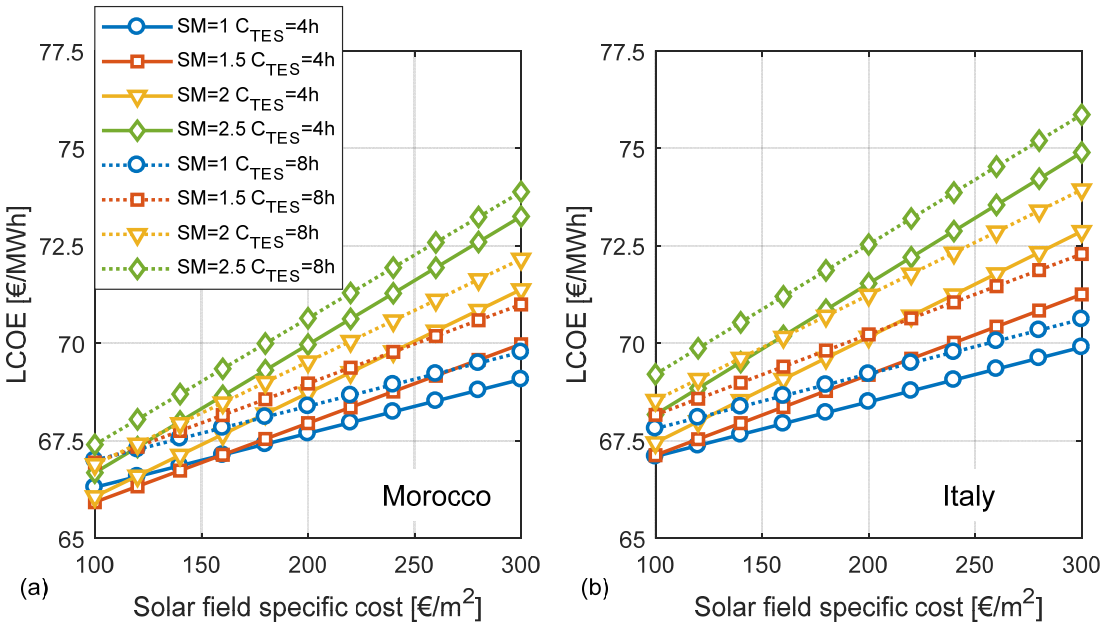

Figure 8 – Levelized cost of energy as function of solar field specific cost using molten salts in case of (a) Moroccan site and (b) Italian site.

6. Conclusions

The paper investigated the benefits arising from the integration of low CO_2 emission steam power plants with concentrating solar systems. Different solar field configurations were studied, varying both collector technology (parabolic trough or linear Fresnel) and heat transfer fluid (direct steam generation or molten salt with thermal energy storage). The achieved results proved that the energy produced by the solar field reduces the efficiency penalty due to CO_2 capture and compression system from about 10.5 percentage point (reference case without solar integration) to a maximum of about 8.5% (ratio between solar energy and fuel chemical energy equal to 0.2). As expected, better performance are achieved in Morocco in comparison to Italian site. The preliminary economic analysis demonstrated as, in Morocco, the solar integration in a USC-PCC plant becomes cost effective for a solar field costs lower than 180 €/m^2 for PTC-DSG case. A reduction of about 60 €/m^2 in solar field cost should occurs for LFC to becomes competitive with PTC solar fields. The use of Molten salts as HTF and the introduction of a TES section enhance the annual energy production but increase the capital and operating costs, resulting less profitable than the direct steam generation.

7. References

[1] Institute for Advanced Sustainability Studies (IASS). IASS Fact Sheet 2/2016 Concentrated Solar Power. 2016.

[2] Mehos M, Turchi C, Vidal J, Wagner M, Ma Z, Ho C, et al. Concentrating solar power: Gen3 demonstration roadmap 2017:1–140.

[3] Siva Reddy V, Kaushik SC, Ranjan KR, Tyagi SK. State-of-the-art of solar thermal power plants - A review. Renew Sustain Energy Rev 2013;27:258–73. doi:10.1016/j.rser.2013.06.037.

[4] Pelay U, Luo L, Fan Y, Stitou D, Rood M. Thermal energy storage systems for concentrated solar power plants. Renew Sustain Energy Rev 2017;79:82–100. doi:10.1016/j.rser.2017.03.139.

[5] Rovira A, Barbero R, Montes MJ, Abbas R, Varela F. Analysis and comparison of Integrated Solar Combined Cycles using parabolic troughs and linear Fresnel reflectors as concentrating systems. Appl Energy 2016;162:990–1000. doi:10.1016/j.apenergy.2015.11.001.

[6] Moghimi MA, Craig KJ, Meyer JP. Simulation-based optimisation of a linear Fresnel collector mirror field and receiver for optical, thermal and economic performance. Sol Energy 2017;153:655–78. doi:10.1016/j.solener.2017.06.001.

[7] Feldhoff JF, Schmitz K, Eck M, Schnatbaum-Laumann L, Laing D, Ortiz-Vives F, et al. Comparative system analysis of direct steam generation and synthetic oil parabolic trough power plants with integrated thermal storage. Sol Energy 2012;86:520–30. doi:10.1016/j.solener.2011.10.026.

[8] Schneider G, Maier H, Stenglein M, Schicktanz P, Stepper R, Schlipf D. Direct Molten Salt Linear Receiver CSP-concepts with MS-TES Compared with Direct Steam Generation Linear Receiver CSP-concepts with Solid Bed TES. Energy Procedia 2015;69:1412–20. doi:10.1016/j.egypro.2015.03.124.

[9] Behar O, Kellaf A, Mohamedi K, Belhamel M. Instantaneous performance of the first integrated solar combined cycle system in Algeria. Energy Procedia 2011;6:185–93. doi:10.1016/j.egypro.2011.05.022.

[10] Pramanik S, Ravikrishna R V. A review of concentrated solar power hybrid technologies. Appl Therm Eng 2017;127:602–37. doi:10.1016/j.applthermaleng.2017.08.038.

[11] Montes MJ, Rovira A, Muñoz M, Martínez-Val JM. Performance analysis of an Integrated Solar Combined Cycle using Direct Steam Generation in parabolic trough collectors. Appl Energy 2011;88:3228–38. doi:10.1016/j.apenergy.2011.03.038.

[12] Nezammahalleh H, Farhadi F, Tanhaemami M. Conceptual design and techno-economic assessment of integrated solar combined cycle system with DSG technology. Sol Energy 2010;84:1696–705. doi:10.1016/j.solener.2010.05.007.

[13] Lim Y, Kim J, Jung J, Lee CS, Han C. Modeling and Simulation of CO2 Capture Process for Coal-based Power Plant Using Amine Solvent in South Korea. Energy Procedia 2013;37:1855–62. doi:10.1016/j.egypro.2013.06.065.

[14] Goto K, Yogo K, Higashii T. A review of efficiency penalty in a coal-fired power plant with post-combustion CO2 capture. Appl Energy 2013;111:710–20. doi:10.1016/j.apenergy.2013.05.020.

[15] Tola V, Pettinau A. Power generation plants with carbon capture and storage: A techno-economic comparison between coal combustion and gasification technologies. Appl Energy 2014;113:1461–74. doi:10.1016/j.apenergy.2013.09.007.

[16] Zhao R, Deng S, Zhao L, Liu Y, Tan Y. Energy-saving pathway exploration of CCS integrated with solar energy: Literature research and comparative analysis. Energy Convers Manag 2015;102:66–80. doi:10.1016/j.enconman.2015.01.018.

[17] Jamel MS, Abd Rahman A, Shamsuddin AH. Advances in the integration of solar thermal energy with conventional and non-conventional power plants. Renew Sustain Energy Rev 2013;20:71–81.

doi:10.1016/j.rser.2012.10.027.
[18] Cau G, Cocco D, Tola V. Performance assessment of USC power plants integrated with CCS and concentrating solar collectors. Energy Convers Manag 2014;88. doi:10.1016/j.enconman.2014.09.040.
[19] Wang F, Zhao J, Li H, Deng S, Yan J. Preliminary experimental study of post-combustion carbon capture integrated with solar thermal collectors. Appl Energy 2017;185:1471–80. doi:10.1016/j.apenergy.2016.02.040.
[20] Cau G, Cocco D, Tola V. Chapter 84 Solar-Assisted Ultra-supercritical Steam Power Plants with Carbon Capture and Storage. Renew. Energy Serv. Mank. Vol II, vol. II, 2016, p. 933–47. doi:10.1007/978-3-319-18215-5.
[21] Zhao Y, Hong H, Zhang X, Jin H. Integrating mid-temperature solar heat and post-combustion CO2-capture in a coal-fired power plant. Sol Energy 2012;86:3196–204. doi:10.1016/j.solener.2012.08.002.
[22] Qadir A, Mokhtar M, Khalilpour R, Milani D, Vassallo A, Chiesa M, et al. Potential for solar-assisted post-combustion carbon capture in Australia. Appl Energy 2013;111:175–85. doi:10.1016/j.apenergy.2013.04.079.
[23] Yang Y, Wang L, Dong C, Xu G, Morosuk T, Tsatsaronis G. Comprehensive exergy-based evaluation and parametric study of a coal-fired ultra-supercritical power plant. Appl Energy 2013;112:1087–99. doi:10.1016/j.apenergy.2012.12.063.
[24] Morin G, Dersch J, Platzer W, Eck M, Häberle A. Comparison of Linear Fresnel and Parabolic Trough Collector power plants. Sol Energy 2012;86:1–12. doi:10.1016/j.solener.2011.06.020.
[25] Forristall R. Heat Transfer Analysis and Modeling of a Parabolic Trough Solar Receiver Implemented in Engineering Equation Solver 2003.
[26] Cau G, Cocco D. Comparison of medium-size concentrating solar power plants based on parabolic trough and linear Fresnel collectors. Energy Procedia 2014;45:101–10. doi:10.1016/j.egypro.2014.01.012.
[27] Bugge J, Kjær S, Blum R. High-efficiency coal-fired power plants development and perspectives. Energy 2006;31:1437–45. doi:10.1016/j.energy.2005.05.025.
[28] P. S. Weitzel, Tanzosh JM, Boring B, Okita N, Takahashi T, Ishikawa N. Advanced Ultra-Supercritical Power Plant (700 to 760C) Design for Indian Coal. J Chem Inf Model 2013;53:1689–99. doi:10.1017/CBO9781107415324.004.
[29] Natesan K, Park JH. Fireside and steamside corrosion of alloys for USC plants. Int J Hydrogen Energy 2007;32:3689–97. doi:10.1016/j.ijhydene.2006.08.038.
[30] Noguchi Y, Okada H, Semba H, Yoshizawa M. Isothermal, thermo-mechanical and bithermal fatigue life of Ni base alloy HR6W for piping in 700??C USC power plants. Procedia Eng 2011;10:1127–32. doi:10.1016/j.proeng.2011.04.186.
[31] Cocco D, Serra F. Performance comparison of two-tank direct and thermocline thermal energy storage systems for 1 MWe class concentrating solar power plants. Energy 2015;81:526–36. doi:10.1016/j.energy.2014.12.067.